A&A 526, A35 (2011)
DOI: 10.1051/0004-6361/201014886

Astronomy & Astrophysics

Asteroseismic modelling of the metal-poor star τ Ceti

Y. K. Tang[1,2] and N. Gai[3,4]

[1] Department of Physics, Dezhou University, Dezhou 253023, PR China
e-mail: tyk450@163.com
[2] Key Lab of Biophysics in Universities of Shandong, Dezhou 253023, PR China
[3] Department of Astronomy, Beijing Normal University, Beijing 100875, PR China
e-mail: gaining@mail.bnu.edu.cn
[4] Department of Astronomy, Yale University, PO Box 208101, New Haven, CT 06520-8101, USA

Received 29 April 2010 / Accepted 6 October 2010

ABSTRACT

Context. Asteroseismology is an efficient tool not only for testing stellar structure and evolutionary theory but also constraining the parameters of stars for which solar-like oscillations are presently detected. As an important southern asteroseismic target τ Ceti, is a metal-poor star. The main features of the oscillations and some frequencies of τ Ceti have been identified. Many scientists propose to comprehensively observe this star as part of the Stellar Observations Network Group.

Aims. Our goal is to obtain the optimal model and reliable fundamental parameters for the metal-poor star τ Ceti by combining all non-asteroseismic observations with these seismological data.

Methods. Using the Yale stellar evolution code (YREC), a grid of stellar model candidates that fall within all the error boxes in the HR diagram have been constructed, and both the model frequencies and large- and small- frequency separations are calculated using the Guenther's stellar pulsation code. The $\chi^2_{\nu c}$ minimization is performed to identify the optimal modelling parameters that reproduce the observations within their errors. The frequency corrections of near-surface effects to the calculated frequencies using the empirical law, as proposed by Kjeldsen and coworkers, are applied to the models.

Results. We derive optimal models, corresponding to masses of about 0.775–0.785 $M_\odot$ and ages of about 8–10 Gyr. Furthermore, we find that the quantities derived from the non-asteroseismic observations (effective temperature and luminosity) acquired spectroscopically are more accurate than those inferred from interferometry for τ Ceti, because our optimal models are in the error boxes B and C, which are derived from spectroscopy results.

Key words. asteroseismology – stars: individual: τ Ceti – stars: oscillations – stars: low-mass

1. Introduction

The solar five-minute oscillations have led to a wealth of information about the internal structure of the Sun. These results have stimulated various attempts to detect solar-like oscillations for a handful of solar-type stars. Solar-like oscillations have been confirmed for several main-sequence, subgiant and red giant stars by the ground-based observations or by the CoRoT and the Kepler space missions, such as ν Indi (Bedding et al. 2006; Carrier et al. 2007), α Cen A (Bouchy & Carrier 2002; Bedding et al. 2004), α Cen B (Carrier & Bourban 2003; Kjeldsen et al. 2005), μ Arae (Bouchy et al. 2005), HD 49933 (Mosser et al. 2005), β Vir (Martić et al. 2004a; Carrier et al. 2005a), Procyon A (Martić et al. 2004b; Eggenberger et al. 2004a; Arentoft et al. 2008; Bedding et al. 2010), η Bootis (Kjeldsen et al. 2003; Carrier et al. 2005b), β Hyi (Bedding et al. 2001, 2007; Carrier et al. 2001), δ Eri (Carrier et al. 2003), 70 Ophiuchi A (Carrier & Eggenberger 2006), ϵ Oph (Ridder et al. 2006), CoRoT target HR7349 (Carrier et al. 2010), KIC 6603624, KIC 3656476 and KIC 11026764 (Chaplin et al. 2010), etc. Furthermore, the large and small frequency separations of p-modes can provide a good estimate of the mean density and age of the stars (Ulrich 1986, 1988). On the basis of these asteroseismic data, numerous theoretical analyses have been performed to determine precise global stellar parameters and test the various complicate physical effects on the stellar structure and evolutionary theory (Thévenin et al. 2002; Eggenberger et al. 2004b, 2005; Kervella et al. 2004; Miglio & Montalbán 2005; Provost et al. 2004, 2006; Tang et al. 2008a,b).

τ Ceti (HR 509, HD 10700) is a G8 V metal-poor star, belonging to population II. Extensive analyses of this star have been performed by many scientists who have provided different non-seismic observational results (such as effective temperature $T_{\rm eff}$ and luminosity L), depending on the different methods used, i.e. interferometry and spectroscopy. Teixeira et al. (2009) detected solar-like oscillations on τ Ceti, identified some possible existing frequencies, and obtained the large separation around $\Delta\nu = 169$ μHz with HARPS. These seismological data will provide a constraint on the fundamental parameters of τ Ceti. Moreover, τ Ceti will be one of the most promising southern asteroseismic targets of the seismology programme of Stellar Observations Network Group (Metcalfe et al. 2010).

In this work, using a mixture of conventional and asteroseismic observed constraints, we try to determine modelling parameters of τ Ceti with YREC. The observational constraints available to τ Ceti are summarized in Sect. 2, while the details of the evolutionary models are presented in Sect. 3. The seismic analyses are carried out in Sect. 4. Finally, the discussion and conclusions are given in Sect. 5.

Table 1. Non-asteroseismic observational data of τ Ceti.

Observable	Value	Source
Effective temperature $T_{\rm eff}$(K)	5264 ± 100	(1)
	5525 ± 12	(3)
Luminosity $L/L_\odot$	0.52 ± 0.03	(4)
	0.50 ± 0.006	(3)
	0.488 ± 0.010	(2)
Metallicity $[Fe/H]_s$	−0.5 ± 0.03	(1)
Surface heavy-element abundance $[Z/X]_S$	0.0073 ± 0.0005	(5)
Radius $R/R_\odot$	0.773 ± 0.024	(5)

References. (1) Soubiran et al. (1998); (2) Teixeira et al. (2009); (3) Pijpers et al. (2003); (4) Pijpers (2003); (5) this paper.

2. Observational constraints

2.1. Non-asteroseismic observational constraints

The metallicity derived from observations is [Fe/H] = −0.5 ± 0.03 (Soubiran et al. 1998). The mass fraction of heavy-elements, Z, was derived assuming log[Z/X] ≈ [Fe/H] + log[Z/X]$_\odot$, and [Z/X]$_\odot$ = 0.0230 (Grevesse & Sauval 1998), for the solar mixture. We can therefore deduce that [Z/X]$_s$ = 0.0068−0.0078. The radius, as an important parameter for constraining stellar models, was first measured by Pijpers et al. (2003) using interferometry. They determined the radius of τ Ceti corresponding to 0.773 ± 0.004$_{(int.)}$ ± 0.02$_{(ext.)}$ $R_\odot$. The measurement of the radius was then improved by Di Folco et al. (2004) and Di Folco et al. (2007). Finally, Di Folco et al. (2007) determined the radius R = 0.790 ± 0.005 $R_\odot$. In our work, we use a large value of radius R = 0.773 ± 0.024 $R_\odot$ which includes all the surrounding observational radius.

The effective temperature and luminosity of τ Ceti are both derived from spectroscopy (5264±100 K and 0.52±0.03 $L_\odot$), and by ensuring that we reproduce the measured radius (5525 ± 12 K, 0.500 ± 0.006 $L_\odot$), using interferometry (Soubiran et al. 1998; Pijpers et al. 2003, Pijpers 2003). In addition the luminosity of a star can be obtained by combining our knowledge of the magnitude and distance. For τ Ceti, the apparent magnitude V = 3.50 ± 0.01, with the revised parallax, gives an absolute magnitude M_V = 5.69 ± 0.01. Teixeira et al. (2009) derived a luminosity for τ Ceti of $L/L_\odot$ = 0.488 ± 0.010, using bolometric correction for τ Ceti B.C. = −0.17 ± 0.02 (Casagrande et al. 2006) and adopting an absolute bolometric magnitude for the Sun of $M_{\rm bol,\odot}$ = 4.74 (Bessel et al. 1998).

Using above different effective temperatures and luminosities, we can obtain three error boxes, which error box A (5525 ± 12 K, 0.50 ± 0.006 $L_\odot$) are denoted by crosses, error box B (5264 ± 100 K, 0.52 ± 0.03 $L_\odot$) denoted by triangles, and error box C (5264 ± 100 K, 0.488 ± 0.010 $L_\odot$) denoted by diamonds, shown in Fig. 1d, respectively. Meanwhile, we decided to increase all errors by a factor of 1.5, so that our calibration of the star is only weakly constrained by these values.

All non-asteroseismic observational constraints are listed in Table 1.

2.2. Asteroseismic constraints

Solar-like oscillations of the G8V star τ Ceti were detected by Teixeira et al. (2009) with the HARPS spectrograph. Thirty-one individual modes are identified (see Table 1 in Teixeira et al. 2009). The large frequency separation is about $\Delta\nu$ = 169 μHz.

Table 2. Input parameters for model tracks.

Variable	Minimum value	Maximum value	δ
Mass $M/M_\odot$	0.770	0.795	0.005
Mixing length α	0.8	1.8	0.2
Initial heavy element abundance Z_i	0.001	0.008	0.0005
Initial hydrogen abundance X_i	0.70	0.75	0.01

Notes. The value δ defines the increment between minimum and maximum parameter values used to create the model array.

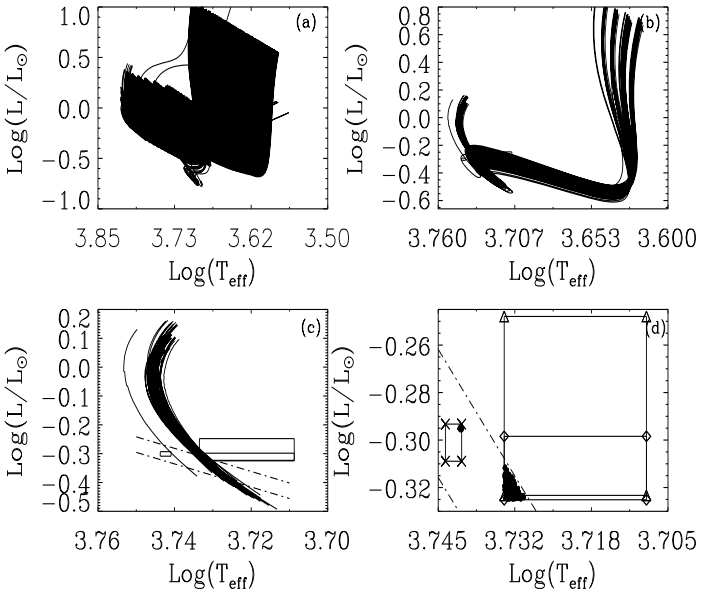

Fig. 1. **a)** All evolutionary tracks in the HR diagram; **b)** Evolutionary tracks falling in the error boxes from pre-main sequence to main sequence; **c)** Blow up the evolutionary tracks falling in the error boxes in the main sequence; **d)** The selected models falling in the error boxes. Error box A (5525 ± 12 K, 0.50 ± 0.006 $L_\odot$) is denoted by crosses, error box B (5264 ± 100 K, 0.52 ± 0.03 $L_\odot$) denoted by triangles, and error box C (5264 ± 100 K, 0.488 ± 0.010 $L_\odot$) denoted by diamonds, respectively.

3. Stellar models

We calculated many evolutionary tracks using Yale stellar evolution code (YREC; Demarque et al. 2008) by inputting different parameters shown in Table 2.

The mass range are M = 0.770–0.795 $M_\odot$ with the increment value 0.005 $M_\odot$. Initial heavy element abundance range are Z_i (0.001–0.008) with the increment value 0.0005 and initial hydrogen abundance X_i (0.70–0.75) with the increment value 0.01. Energy transfer by convection is treated according to the standard mixing-length theory, and the boundaries of the convection zones are determined by the Schwarzschild criterion (see Demarque et al. 2008, for details of the YREC). We set the mixing length parameter α = 0.8–1.8 with the increment value 0.2. Using these parameter space, we created the model array. The initial zero-age main sequence (ZAMS) model used for τ Ceti is created from pre-main-sequence evolution calculations. These models are calculated using the updated OPAL equation-of-state tables EOS2005 (Rogers & Nayfonov 2002). We used OPAL high temperature opacities (Iglesias & Rogers 1996)

Table 3. The observational frequencies and the theoretical frequencies for model M1 & M2 before and after correction for near-surface offset, respectively.

					Before		Correction					
	Observational	Frequencies			Model	M1				Model	M2	
n	$l=0$	$l=1$	$l=2$	$l=3$	$l=0$	$l=1$	$l=2$	$l=3$	$l=0$	$l=1$	$l=2$	$l=3$
18	3293.4	...	...	...	3296.149	3377.700	3455.831	3529.092	3296.276	3377.775	3455.826	3529.043
19	3461.7	...	...	3692.9	3465.623	3547.268	3625.910	3699.994	3465.717	3547.304	3625.854	3699.900
20	3634.5	...	...	3863.7	3635.309	3717.485	3796.205	3870.802	3635.352	3717.479	3796.119	3870.664
21	3799.3	3885.3	...	4030.3	3805.155	3887.715	3967.112	4042.136	3805.169	3887.661	3966.987	4041.970
22	3976.1	4046.8	4126.1	4202.5	3975.695	4058.363	4138.126	4213.984	3975.674	4058.279	4137.957	4213.769
23	4139.9	4222.7	4298.2	...	4146.398	4229.665	4309.760	4385.981	4146.331	4229.535	4309.557	4385.721
24	...	4388.3	4469.5	4545.1	4317.694	4401.101	4481.820	4558.582	4317.594	4400.922	4481.566	4558.284
25	4481.8	...	...	...	4489.499	4573.112	4653.968	4731.322	4489.349	4572.896	4653.669	4730.972
26	4652.3	...	4811.8	...	4661.385	4745.381	4826.607	4904.208	4661.190	4745.115	4826.269	4903.817
27	4816.2	4903.1	...	5060.5	4833.772	4917.748	4999.286	5077.435	4833.537	4917.439	4998.898	5077.001
28	...	5072.3	5151.8	...	5006.247	5090.515	5172.103	5250.549	5005.962	5090.165	5171.678	5250.071
29	...	5240.0	5317.5	...	5178.835	5263.220	5345.147	5423.822	5178.510	5262.825	5344.685	5423.311
30	...	5411.2	5492.8	...	5351.685	5436.051	5518.036	5597.086	5351.322	5435.623	5517.539	5596.541
31	5497.9	...	...	...	5524.391	5608.945	5691.011	5770.097	5523.990	5608.485	5690.491	5769.528
					After		Correction					
18	3293.4	...	...	...	3294.811	3373.293	3448.558	3521.990	3294.873	3373.414	3448.676	3522.028
19	3461.7	...	...	3692.9	3463.687	3542.188	3617.891	3692.166	3463.725	3542.282	3617.973	3692.180
20	3634.5	...	...	3863.7	3632.637	3711.616	3787.344	3862.157	3632.638	3711.682	3787.412	3862.151
21	3799.3	3885.3	...	4030.3	3801.588	3880.925	3957.295	4032.565	3801.579	3880.961	3957.344	4032.561
22	3976.1	4046.8	4126.1	4202.5	3971.050	4050.500	4127.228	4203.364	3971.028	4050.527	4127.255	4203.345
23	4139.9	4222.7	4298.2	...	4140.467	4220.554	4297.635	4374.174	4140.428	4220.560	4297.652	4374.152
24	...	4388.3	4469.5	4545.1	4310.239	4390.548	4468.303	4545.430	4310.201	4390.534	4468.298	4545.417
25	4481.8	...	...	...	4480.250	4560.894	4638.878	4716.651	4480.204	4560.877	4638.861	4716.641
26	4652.3	...	4811.8	...	4650.045	4731.252	4809.736	4887.824	4650.003	4731.224	4809.718	4887.837
27	4816.2	4903.1	...	5060.5	4820.001	4901.433	4980.409	5059.120	4819.977	4901.408	4980.383	5059.162
28	...	5072.3	5151.8	...	4989.674	5071.706	5150.968	5230.066	4989.668	5071.692	5150.953	5230.148
29	...	5240.0	5317.5	...	5159.046	5241.582	5321.475	5400.908	5159.079	5241.584	5321.477	5401.051
30	...	5411.2	5492.8	...	5328.222	5411.212	5491.524	5571.452	5328.308	5411.249	5491.552	5571.669
31	5497.9	...	...	...	5496.757	5580.498	5661.325	5741.433	5496.908	5580.579	5661.397	5741.746

supplemented with low temperature opacities from Ferguson et al. (2005). The NACRE nuclear reaction rates (Angulo et al. 1999) were used. The Krishna-Swamy Atmosphere T-τ relation is used for solar-like star (Guenther & Demarque 2000). All models included gravitational settling of helium and heavy elements using the formulation of Thoul et al. (1994).

Figure 1a shows that many evolutionary tracks cover all possible evolutionary status of τ Ceti. According to the above four error boxes, we select all the tracks crossing the error boxes shown in Fig. 1b. We only choose to study main-sequence models, which are shown in Fig. 1c. Meanwhile, we use the mass and radius to estimate the large separation according to Eq. (1) (Kjeldsen & Bedding 1995; Miglio et al. 2009a,b). Furthermore, using the temperature, luminosity, radius, and larger separation (refer to the values from Teixeira et al. 2009) as constrainst, we select the models of τ Ceti provided in Fig. 1d as candidates.

$$\Delta\nu = \sqrt{\frac{M/M_\odot}{(R/R_\odot)^3}} \times 134.9\,\mu\mathrm{Hz}. \quad (1)$$

We now consider a function that describes the agreement between the observations and the theoretical results

$$\chi^2_1 = \frac{1}{5}\sum_{i=1}^{5}\left(\frac{C_i^{\mathrm{theo}} - C_i^{\mathrm{obs}}}{\sigma C_i^{\mathrm{obs}}}\right)^2, \quad (2)$$

where $\boldsymbol{C}$ represents the quantities $L/L_\odot$, T_{eff}, $R/R_\odot$, and $[\mathrm{Fe/H}]_s$ and large frequency separation $\Delta\nu$, $\boldsymbol{C}^{\mathrm{theo}}$ represents the theoretical values, and $\boldsymbol{C}^{\mathrm{obs}}$ represents the observational values listed in Table 1. The vector $\sigma\boldsymbol{C}_i^{\mathrm{obs}}$ contain the errors in these observations, which are also given in Table 1. We also decided to adopt a large error (all errors are increased by a factor of 1.5), so that our calibration of the star is only weakly constrained by these values, which is not precisely determined. Figure 2a presents the values χ^2_1 versus age t of selected models that are shown in Fig. 1d. We find that we cannot select an optimal model from Fig. 2a. From Fig. 2a, we find that it is difficult to select an optimal model depending mainly on the non-seismic constraints and $\Delta\nu$, which was estimated by simply scaling from solar value using Eq. (1). Hence, a detailed pulsation analysis are needed in the next step.

4. Asteroseismic constraints of fundamental parameters

Using Guenther's pulsation code (Guenther 1994), we calculate the adiabatic low-l p-mode frequencies, the large- and small- frequency separations ($\Delta\nu_{n,l} \equiv \nu_{n,l} - \nu_{n-1,l}$ and $\delta\nu_{n,l} \equiv \nu_{n,l} - \nu_{n-1,l+2}$, defined by Tassoul 1980) of all the selected models. We compare

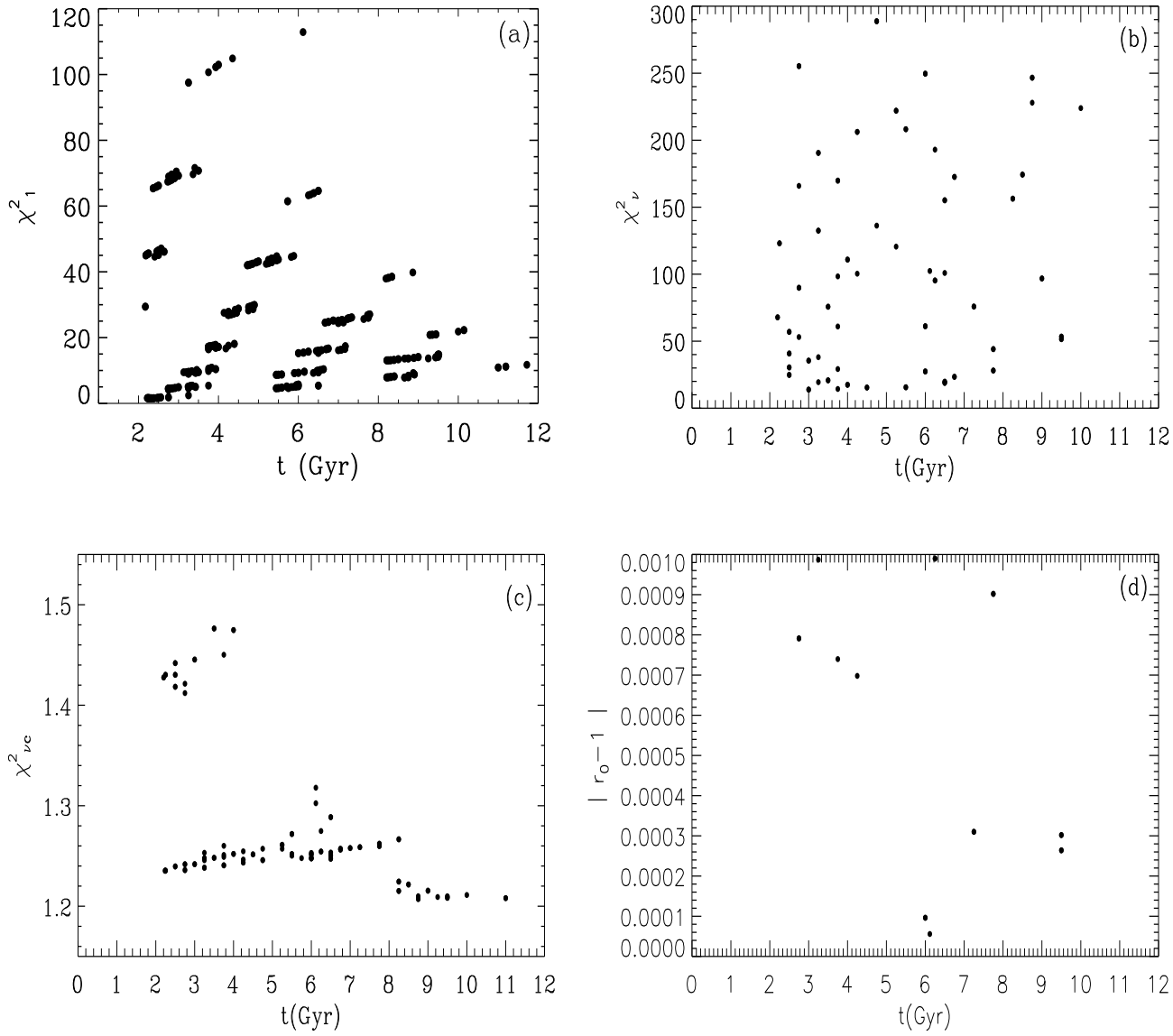

Fig. 2. **a)** χ^2_1 values derived from Eq. (2), plotted as a function of age; **b)** χ^2_ν values derived from Eq. (3), plotted as a function of age; **c)** $\chi^2_{\nu c}$ values derived from Eq. (6), plotted as a function of age; **d)** $|r_0 - 1|$ values plotted as a function of age.

the theoretical frequencies with the corresponding observational frequencies using the function χ^2_ν

$$\chi^2_\nu = \frac{1}{N}\sum_{n,l}\left(\frac{\nu_l^{\rm theo}(n) - \nu_l^{\rm obs}(n)}{\sigma}\right)^2, \quad (3)$$

where, $N = 31$ is the total number of modes, and $\nu_l^{\rm theo}(n)$ and $\nu_l^{\rm obs}(n)$ are the theoretical and observed frequencies respectively, for each spherical degree l and the radial order n, where $\sigma = 2$ μHz (Teixeira et al. 2009) represents the uncertainty in the observed frequencies and χ^2_ν values, plotted as function of age, are shown in Fig. 2b.

Since existing stellar models fail to accurately represent the near-surface layers of the solar-like stars, where the turbulent convection take place, the systematic offset between the observed and model frequencies appears. Furthermore, this offset between observed and best model frequencies turns out to be closely fitted by a power law (Christensen-Dalsgaard & Gough 1980; Kjeldsen et al. 2008; Metcalfe et al. 2009; Doğan et al. 2009, 2010; Bedding et al. 2010; Christensen-Dalsgaard et al. 2010). In other words, this offset increases with increasing frequency shown in Fig. 3. This power law can be expressed using the equation

$$\nu_{\rm obs}(n) - r_l\nu_{\rm theo}(n) = a_l[\nu_{\rm obs}(n_i)/\nu_{\rm max}]^b, \quad (4)$$

where $\nu_{\rm obs}$ are the observed frequencies of radial and non-radial order, $\nu_{\rm best} = r_l\nu_{\rm theo}(n)$ are the corresponding calculated frequencies of the best-fit model, and $\nu_{\rm max}$ is a constant frequency corresponding to the peak power in the spectrum, which is taken as 4490 μHz for τ Ceti and r_l, a_l, and b are parameters described in detail by Kjeldsen et al. (2008), (for a different spherical degree l, the values of r and a are denoted by r_l and a_l, respectively). For the Sun and a solar-like star, the exponent $b = 4.90$ is appropriate, as has been proven by many scientists. We use

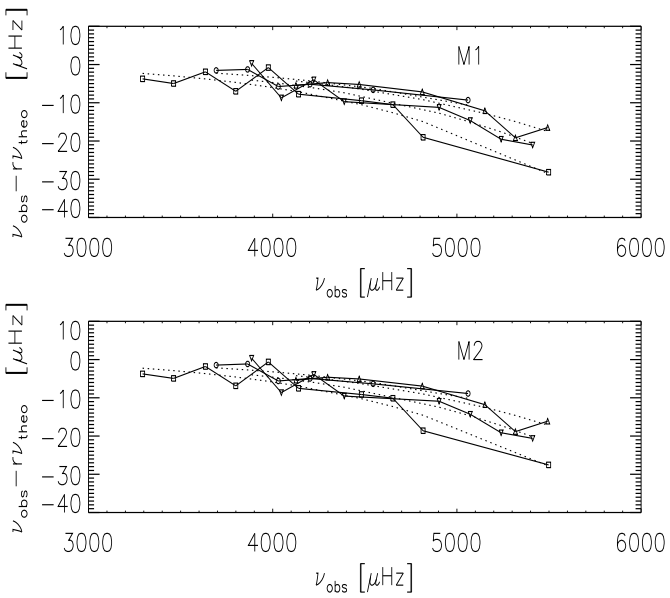

Fig. 3. The difference between observed and best-fit model frequencies, according to the left term of Eq. (4). Squares are used for $l = 0$ modes, diamonds for $l = 1$ modes, triangles for $l = 2$ modes, and circles for $l = 3$. Dotted lines show the power-law function, according to the right term of Eq. (4).

the Kjeldsen et al. (2008) prescription to correct the theoretical frequencies from near surface effects.

According to Eq. (4), we can use the following equation to obtain the corrected frequencies of models:

$$\nu_{\rm correct}(n) = r_l \nu_{\rm theo}(n) + a_l [\nu_{\rm obs}(n)/\nu_{\rm max}]^b. \quad (5)$$

We define the function $\chi^2_{\nu c}$ in a similar way to Eq. (3) as

$$\chi^2_{\nu c} = \frac{1}{N} \sum_{n,l} \left(\frac{\nu_l^{\rm correct}(n) - \nu_l^{\rm obs}(n)}{\sigma(\nu_l^{\rm obs}(n))} \right)^2. \quad (6)$$

The values of $\chi^2_{\nu c}$, plotted as a function of age are shown in Fig. 2c. From Fig. 2c, we can see that the values of $\chi^2_{\nu c}$ are lower than χ^2_ν and their lowest values correspond to model ages from 8 to 10 Gyr. We conclude that the optimal model corresponds to the lower values of χ^2_ν and $r_0 - 1$. From Figs. 2c and 2d, we infer that only two models M1 and M2 can be accurately described by the observational constraints. The difference between the observed and uncorrected model frequencies of M1 and M2 are shown in Fig. 3. The uncorrected and corrected frequencies of the optimal models M1 and M2 and the observational frequencies are shown in Table 3.

To clearly compare all of the theoretical frequencies of the models with observational frequencies, we provide echelle diagrams of models M1 and M2 in Fig. 4. An Echelle diagram is a useful tool for comparing stellar models with observations. This diagram presents the mode frequencies along the ordinate axis, and the same frequencies modulo the large separations in abscissae. From Figs. 4a and 4d, it can be seen that the uncorrected theoretical frequencies are not closely in agreement with the observed frequencies. The corrected theoretical frequencies indicated by Eq. (5) fit perfectly the observation shown in Figs. 4b and 4e. Because the observed frequencies of orders n are not consecutive and the values of $\nu_{\rm obs}(n)$ are very close to those of $\nu_{\rm theo}(n)$, we substitute the $\nu_{\rm theo}(n)/\nu_{\rm max}$ for $\nu_{\rm obs}(n)/\nu_{\rm max}$. Hence Eq. (5) becomes

$$\nu_{\rm correct}(n) = r\nu_{\rm theo}(n) + a[\nu_{\rm theo}(n)/\nu_{\rm max}]^b. \quad (7)$$

Table 4. Final model-fitting results for τ Ceti.

Modelling parameters	Model M1	Model M2
Mass $M/M_\odot$	0.775	0.785
Mixing length α	1.6	1.6
Z_i	0.007	0.007
X_i	0.740	0.750
Model characteristics		
Effective temperature $T_{\rm eff}$(K)	5409	5387
Luminosity $L/L_\odot$	0.47985	0.47612
Log (g)	4.53187	4.53365
Radius $R/R_\odot$	0.78994	0.79339
$(Z/X)_{\rm s}$	0.00753	0.00749
Age (Gyr)	9.5	9.5
$\langle\Delta\nu_0\rangle$ (μHz)	170.9222	170.9106
$\langle\Delta\nu_1\rangle$ (μHz)	170.8621	170.8381
$\langle\Delta\nu_2\rangle$ (μHz)	171.0555	171.0332
$\langle\Delta\nu_3\rangle$ (μHz)	171.5120	171.4870
$\langle\delta\nu_{02}\rangle$ (μHz)	10.013	10.111
$\langle\delta\nu_{13}\rangle$ (μHz)	18.034	18.136
Model corrected paraments		
r_0	1.000302	1.000264
r_1	0.9993002	0.9993007
r_2	0.9984142	0.9984387
r_3	0.9984967	0.9984996
a_0	–10.59438	–10.32439
a_1	–8.270579	–8.092409
a_2	–6.517972	–6.377440
a_3	–5.891401	–5.639216

From Figs. 4b, 4c, 4e, and 4f, it can be seen that corrected frequencies given by Eqs. (5) and (7) respectively are uniform and reproduce the observed frequencies perfectly. Furthermore, we can use the function $\chi^2_{\nu c}$ to select the fitting model parameters. As we all know, the suitable model parameters correspond to the lowest values of $\chi^2_{\nu c}$, which can be clearly seen in Fig. 5. From Fig. 5, we can conclude that the mass is in the range 0.775–0.785 $M_\odot$, α is in the range 1.6–1.8, Z_i in 0.0065–0.0075, and X_i 0.73–0.75. Hence, the model parameters of τ Ceti can be constrained to within these narrow ranges. Finally, we list the model parameters and characteristics of models M1 and M2 in Table 4.

5. Discussion and conclusions

Using the asteroseismic analysis and the empirical frequency correction for the near-surface offset presented by Kjeldsen et al. (2008) to correct our theoretical frequencies, we have derived the optimal model of τ Ceti and now list our main conclusions:

1. Using the latest asteroseismic observations, we have attempted to construct the optimal model of τ Ceti. We have only considered the models M1 and M2 , which can closely describe the observations, as the optimal models. Furthermore, the model parameters of τ Ceti have been constrained to within narrow intervals by the function $\chi^2_{\nu c}$, where the mass is in the range $M = 0.775$–$0.785\ M_\odot$, the mixing length parameter in the range $\alpha = 1.6$–1.8, the initial metallicity in the range $Z_i = 0.0065$–0.0075, the initial hydrogen abundance in the range $X_i = 0.73$–0.75, and the age in the range $t = 8$–10 Gyr.

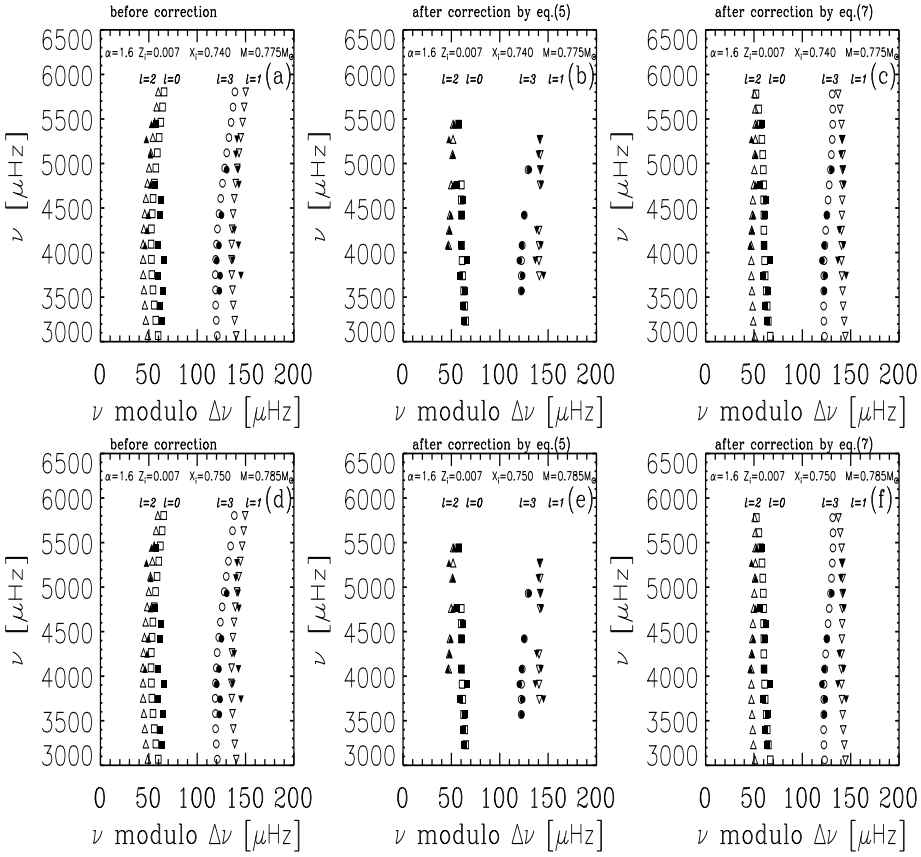

Fig. 4. Echelle diagrams for the optimal models M1 (*upper panel*) and M2 (*lower panel*). *Left panel shows* the case before applying near-surface corrections. *Middle panel* shows the case after applying near-surface corrections, according to Eq. (5). *Right panel* shows the case after applying near-surface corrections, according to Eq. (7). Open symbols refer to the theoretical frequencies, and filled symbols refer to the observable frequencies. Squares are used for $l = 0$ modes, diamonds for $l = 1$ modes, triangles for $l = 2$ modes, and circles for $l = 3$. The observable frequencies correspond to the average large separation about 170 μHz (see text for details).

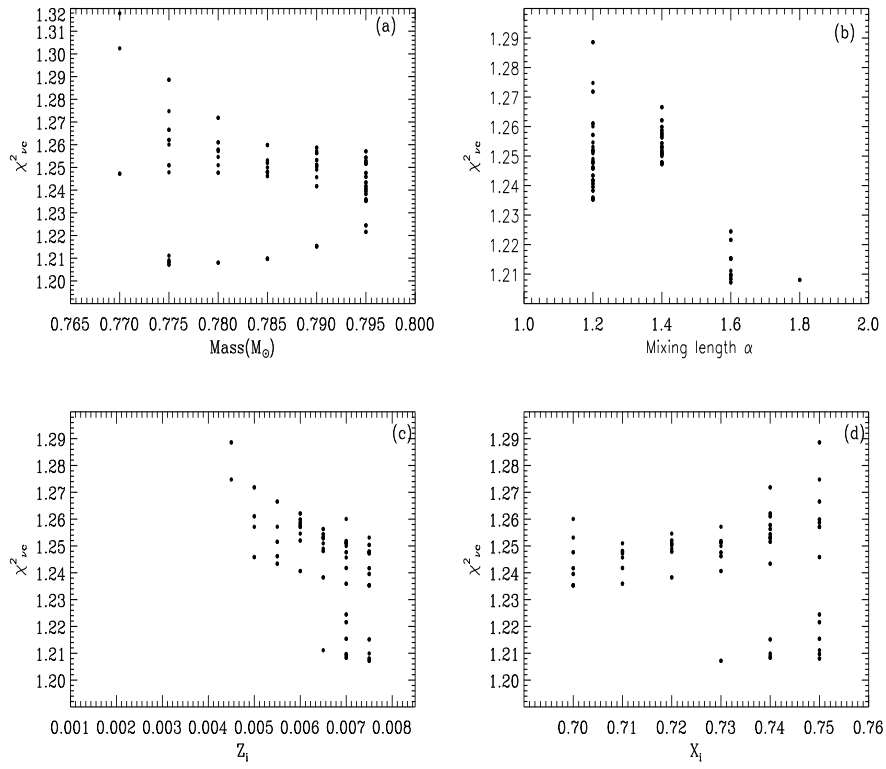

Fig. 5. **a)** $\chi^2_{\nu c}$ values derived from Eq. (6), plotted as function of mass; **b)**. $\chi^2_{\nu c}$ values plotted as function of mixing length α; **c)**. $\chi^2_{\nu c}$ values plotted as function of initial heavy element abundance Z_i; **d)**. $\chi^2_{\nu c}$ values plotted as function of initial hydrogen abundance X_i.

2. We have found that the results of the non-asteroseismic observations (effective temperature and luminosity) inferred from spectroscopy are more accurate than those derived from interferometry for τ Ceti, because our optimal models are in the error boxes B and C derived from our spectroscopy results.

Acknowledgements. We are grateful to the anonymous referee for his/her constructive suggestions and valuable remarks that helped us to improve the manuscript. We also thank Professor Shaolan Bi and Dr. Linghuai Li for many useful comments and discussions. This work was supported by the support of Shandong Nature Science Foundation (ZR2009AM021), Dezhou University Foundation(402811), and supported by The Ministry of Science and Technology of the Peoples Republic of China through grant 2007CB815406, and by NSFC grants 10773003, 10933002, and 10978010.

References

Arentoft, T., Kjeldsen, H., Bedding, T. R., et al. 2008, ApJ, 687, 1080
Angulo, C., Arnould, M., Rayet, M., et al. 1999, Nucl. Phys. A., 656, 3
Bessell, M. S., Castelli, F., & Plez, B. 1998, A&A, 333, 231
Bedding, T. R., Butler, R. P., Kjeldsen, H., et al. 2001, ApJ, 549, L105
Bedding, T. R., Kjeldsen, H., Butler, R. P., et al. 2004, ApJ, 614, 380
Bedding, T. R., Butler, R. P., Carrier, F., et al. 2006, ApJ, 647, 558
Bedding, T. R., Kjeldsen, H., Arentoft, T., et al. 2007, ApJ, 663, 1315
Bedding, T. R., Kjeldsen, H., Campante, T. L., et al. 2010, ApJ, 713, 935
Bouchy, F., & Carrier, F. 2002, A&A, 390, 205
Bouchy, F., Bazot, M., Santos, N. C., Vauclair, S., & Sosnowska, D. 2005, A&A, 440, 609
Bruntt, H., Bedding, T. R., Quirion, P.-O., et al. 2010, MNRAS, 405, 1907
Brown, T. M., Gilliland, R. L., Noyes, R. W., & Ramsey, L. W. 1991, A&A, 368, 599
Carrier, F., & Bourban, G. 2003, A&A, 406, L23
Carrier, F., & Eggenberger, P. 2006, A&A, 450, 695
Carrier, F., Bouchy, F., Kienzle, F., et al. 2001, A&A, 378, 142
Carrier, F., Bouchy, F., & Eggenberger, P. 2003, in Asteroseismology Across the HR Diagram, ed. M. J. Thompson, M. S. Cunha, & M. J. P. F. G. Monteiro (Kluwer), 311
Carrier, F., Eggenberger, P., D'Alessandro, A., & Weber, L. 2005a, New Astron., 10, 315
Carrier, F., Eggenberger, P., & Bouchy, F. 2005b, A&A, 434, 1085
Carrier, F., Kjeldsen, H., Bedding, T. R., et al. 2007, A&A, 470, 1059
Carrier, F., Morel, T., Miglio, A., et al. 2010, Ap&SS, 328, 83
Casagrande, L., Portinari, L., & Flynn, C. 2006, MNRAS, 373, 13
Christensen-Dalsgaard, J., & Gough, D. O. 1980, Nature, 288, 544
Christensen-Dalsgaard, J., Kjeldsen, H., Brown, T. M., et al. 2010, ApJ, 713, L164
Chaplin, W. J., Appourchaux, T., Elsworth, Y., et al. 2010, ApJ, 713, L169
Demarque, P., Guenther, D. B., Li, L. H., et al. 2008, Ap&SS, 316, 31
De Ridder, J., Barban, C., Carrier, F., et al. 2006, A&A, 448, 689
Di Folco, E., Thvenin, F., Kervella, P., et al. 2004, A&A, 426, 601
Di Folco, E., Absil, O., Augereau, J.-C., et al. 2007, A&A, 475, 243
Doğan, G., Brandão, I. M., Bedding, T. R., et al. 2009, Ap&SS, 328, 101
Doğan, G., Bonanno, A., & Christensen-Dalsgaard, J. 2010, appear in the HELAS IV International Conference proceedings in Astronomische Nachrichten
Eggenberger, P., Carrier, F., Bouchy, F., & Blecha, A. 2004a, A&A, 422, 247
Eggenberger, P., Charbonnel, C., Talon, S., et al. 2004b, A&A, 417, 235
Eggenberger, P., Carrier, F., & Bouchy, F. 2005, New Astron., 10, 195
Eggenberger, P., Miglio, A., Carrier, F., et al. 2008, A&A, 482, 631
Ferguson, J. W., Alexander, D. R., Allard, F., et al. 2005, ApJ, 623, 585
Gai, N., Bi, S. L., & Tang, Y. K. 2008, ChJAA, 8, 591
Gray, D. F., & Baliunas, S. L. 1994, ApJ, 427, 1042
Grevesse, N., & Sauval, A. J. 1998, SSRv, 85, 161
Guenther, D. B. 1994, ApJ 422, 400
Guenther, D. B., & Demarque, P. 2000, ApJ, 531, 503
Guenther, D. B., Demarque, P., Kim, Y.-C., et al. 1992, ApJ, 387, 372
Iglesias, C. A., & Rogers, F. J. 1996, ApJ, 464, 943
Judge, P. G., Saar, S. H., Carlsson, M., & Ayres, T. R. 2004, ApJ, 609, 392
Kallinger, T., Weiss, W. W., Barban, C., et al. 2010, A&A, 509, A77
Kervella, P., Thévenin, F., Morel, P., et al. 2004, A&A, 413, 251
Kjeldsen, H., & Bedding, T. R. 1995, A&A, 293, 87
Kjeldsen, H., Bedding, T. R., Baldry, I. K., et al. 2003, AJ, 126, 1483
Kjeldsen, H., Bedding, T. R., Butler, R. P., et al. 2005, ApJ, 635, 1281
Kjeldsen, H., Bedding, T. R., & Christensen-Dalsgaard, J. 2008, ApJ, 683, L175
Li, L. H., Robinson, F. J., Demarque, P., Sofia, S., & Guenther, D. B. 2002. ApJ, 567, 1192
Martić, M., Lebrun, J.-C., Appourchaux, T., & Korzennik, S. G. 2004a, A&A, 418, 295
Martić, M., Lebrun, J. C., Appourchaux, T., & Schmitt, J. 2004b, in SOHO 14/GONG 2004 Workshop, Helio- and Asteroseismology: Towards a Golden Future, ed. D. Danesy, ESA SP-559, 563
Metcalfe, T. S., Creevey, O. L., & Christensen-Dalsgaard, J. 2009, ApJ, 699, 373
Metcalfe, T. S., Judge, P. G., Basu, S., et al. 2010, AAS Meeting 215, 424.16
Miglio, A., & Montalbán, J. 2005, A&A, 441, 615
Miglio, A., Montalbán, J., Eggenberger, P., et al. 2009a, AIP Conf. Proc., 1170, 132
Miglio, A., Montalbán, J., Baudin, F., et al. 2009b, A&A, 503, L21
Mosser, B., Bouchy, F., Catala, C., et al. 2005, A&A, 431, L13
Pijpers, F. P. 2003, A&A, 400, 241
Pijpers, F. P., Teixeira, T. C., Garcia, P. J., et al. 2003, A&A, 406, L15
Provost, J., Martic, M., & Berthomieu, G. 2004, ESA SP-559, 594
Provost, J., Berthomieu, G., Martić, M., & Morel, P. 2006, A&A, 460, 759
Rogers, F. J., & Nayfonov, A. 2002, ApJ, 576, 1064
Robinson, F. J., Demarque, P., Li, L. H., et al. 2003, MNRAS, 340, 923
Samadi, R., Georgobiani, D., Trampedach, R., et al. 2007, A&A, 463, 297
Soubiran, C., Katz, D., & Cayrel, R. 1998, A&AS, 133, 221
Stello, D., Chaplin, W. J., Basu, S., et al. 2010, MNRAS, 400, L80
Tang, Y. K., Bi, S. L., Gai, N., et al. 2008a, ChJAA, 8, 421
Tang, Y. K., Bi, S. L., & Gai, N. 2008b, New Astron., 13, 541
Tassoul, M. 1980, ApJS, 43, 469
Teixeira, T. C., Kjeldsen, H., Bedding, T. R., et al. 2009, A&A, 494, 237
Thévenin, F., Provost, J., Morel, P., et al. 2002, A&A, 392, 9
Thoul, A. A., Bahcall, J. N., & Loeb, A. 1994, ApJ 421, 828